Automated Multi- and Block-Copolymer Writing in Mesoporous Films Using Visible-Light PET-RAFT and a Microscope

*Claire Förster, Robert Lehn, and Annette Andrieu-Brunsen**

For high throughput applications, e.g., in the context of sensing especially when being combined with machine learning, large sample numbers in acceptable production time are required. This needs automated synthesis and material functionalization concepts ideally combined with high precision. To automate sensing relevant mesopore polymer functionalization while being highly precise in polymer placement, polymer amount control, and polymer sequence design, a process for polymer writing in mesoporous silica films with pore diameter in the range of 13 nm is developed. Mesoporous films are functionalized with different polymers in adjustable polymer amount including block-copolymer functionalization in an automated process using a visible-light induced, controlled photo electron/energy transfer- reversible addition-fragmentation chain-transfer (PET-RAFT) polymerization. While transferring this PET-RAFT to a commercially available microscope, direct, automated laser writing of three different polymers, as well as polymer re-initiation is demonstrated. Using a laser diameter of ≈72 μm, significantly smaller polymer spots of ≈7 μm in diameter are realized. Micrometerscale resolved polymer images including block-copolymers are written into mesoporous layers covering millimeter scale areas requiring a writing time in the range of one second per polymer spot.

1. Introduction

The ability to automate chemical synthesis is relevant not only for material fabrication itself, but also for Lab on a Chip and sensor devices[1] and especially for generating sufficiently large datasets which can be combined with machine learning concepts.[2] An increasing trend toward automation is observed in synthesis and in applications.[3] For example, high throughput concepts, particularly known from screening of large libraries in medical applications, were applied to synthesis, e.g., in controlled living/radical polymerization.[4,5] Thereby, automated polymer synthesis mostly refers to parallel methods using synthetic robots,[6] for optimization of reaction condition and design of new materials.[4]

Structured surface functionalization has been less automated and automated polymer functionalization in nanopores including the ability to locally control polymer functionalization at the micrometer and nanometer scale while designing the local polymer chain composition and polymer pattern in an automated and individualized manner is still a challenge. Polymer (local) placement on surfaces are usually generated using photolithography or microcontact printing[7] in which specific areas of a surface can be polymer functionalized by exposure to (UV-) light. Using photomasks, many replicates of the same pattern can be generated in a short time, whereby flexibility in image or pattern variant generation is limited to the applied mask. Thereby, a majority of photopolymerizations have been applied to photolithography. In this context, automated oxygen tolerant controlled radical polymerizations[4,8] as well as, the use of visible-light induced polymerizations are advantageous and are increasingly investigated as they can be combined with suitable laser wavelengths and ambient conditions.[9,10] Furthermore, local functionalization without photomasks has also been demonstrated at planar surfaces, including techniques allowing for higher resolution than traditional photomask-based photolithography like dip-pen lithography.[11] Many of these techniques, including dip-pen lithography, are relatively slow and often limited to planar surfaces. Mask-less local functionalization, using visible light, was realized by using a laser as light source and to structure polymer materials on surfaces as well as in three dimensions starting from a planar surface. While using one photon polymerization processes microstructured polymer functionalization was demonstrated.[12] Using direct laser writing (DLW) at planar surfaces highly precise surface functionalization, in micron to even tens of nanometer resolution has been demonstrated using digital control of the laser beam and multi-photon adsorption processes.[13,14] DLW which is based on two- or multi-photon absorption is mostly applied in the context of 3D structuring

C. Förster, R. Lehn, A. Andrieu-Brunsen
Macromolecular Chemistry - Smart Membranes
Technische Universität Darmstadt
64287 Darmstadt, Germany
E-mail: brunsen@cellulose.tu-darmstadt.de

**ADVANCED
SCIENCE NEWS**

www.advancedsciencenews.com

**NANO · MICRO
small**

www.small-journal.com

and additive manufacturing, using a film of pre-polymer resin which is thicker than the designed structure height.[15] The focus of DLW primarily lies on the production of precise 3D structures on the micrometer scale on planar surfaces and is mostly limited to homopolymer structures. The combination of DLW with stimulated emission depletion (STED) allowed to overcome the resolution limit due to refraction of traditional DLW.[16]

It has to be noted, that mask-less photilithography and nanolithography is usually based on visible-light irradiation and thus needs visible-light initiated polymerizations. In case of two-photon DLW the photoinitiators, as well as the monomer/oligomer needs to be transparent at the used laser wavelength.[14] Many photoresists used for DLW are based on free radical photopolymerizations.[14,17] A combination of laser writing with a controlled radical polymerization was reported by Soppera and colleagues.[18,19] Using nitroxide mediated photo-polymerization (NMP2) a cross-linked polymer film bearing nitroxide moieties on a silica surface was obtained. The subsequent polymer functionalization by re-initiation was performed using a free radical polymerization under UV light.[18] The same NMP2 process was demonstrated to allow re-initiation and multiple functionalization using two different monomers by DLW.[19] Tang et al.[20] used a ring opening metathesis polymerization (ROMP) to generate poly(barrelene-*co*-norbornene) films, which were further patterned by dehydrogenation using DLW. Wu et al.[21] demonstrated 3D DLW using a photo-mediated RAFT polymerization for the first time, obtaining microstructures with feature sizes of ≈500 nm using macro-photo-iniferter synthesized by RAFT polymerization. The DLW was carried out using different monomers, such as pentaerythiritol triacrylate (PETA), trimethylolpropane triacrylate (TMPTA), and *N*-isopropylacrylamide (NIPAM), and these monomers were also demonstrated to perform re-initiation. The group of Lalevée[22] achieved re-initiation using DLW: After preparing a polymer layer on a planar microscope coverslide a second monomer was polymerized on top using a digitally controlled laser beam at a wavelength of 532 nm. In this context 780 or 800 nm light is mostly used together with a two photon initiation process.[14] Using laser writing, even a direct self-assembly of block copolymer films was reported.[23] Besides the few examples of controlled polymerization techniques combined with laser writing many more visible-light induced controlled polymerizations have been developed mostly as solution polymerization[24] within the past decade including RAFT,[25] atom transfer rdical polymerization (ATRP),[26] ionic,[27] and ROM polymerizations.[28] For polymer writing using laser light, robust reaction conditions including water and oxygen tolerance as well as ambient temperature, and short reaction times are required. In 2014 the group of Boyer developed the photoinduced electron/energy transfer (PET)-RAFT,[29] which allows ambient reaction conditions due to the oxygen tolerance under the use of visible-light irradiation. This PET-RAFT can be carried out at different wavelengths depending on selected photo catalysts. Often transition metals, such as tris(bipyridine) ruthenium(II) chloride (Ru(bpy)$_3$Cl$_2$),[29] or zinc tetraphenyl-porphyrin (ZnTPP),[25,30] are used, but also organic molecules like Eosin Y and fluorescein can be used as photo catalysts.[31] Furthermore, Shanmugam et al. used bacteriochlorophyll as a

photocatalyst and demonstrated the first PET-RAFT under near-infrared/far-red irradiation (850 and 780 nm).[32] Kurek et al. investigated the influence of reaction conditions on the PET-RAFT. Light intensity, catalyst, and chain transfer agent (CTA) amount seem to have the major influence on the kinetics[33] although the exact mechanism is still under debate.[40] Very interestingly only few examples on porous and especially on mesoporous material functionalization using PET-RAFT exist.[34,35]

Here, we successfully demonstrate DLW and automated polymer writing inside mesoporous silica thin films. Millimeter area polymer and block-copolymer images with a few micrometer local resolution using 405 nm laser and a PET-RAFT polymerization into nanoscale pores were achieved. The automated and customized locally resolved writing of varying polymer type and polymer amount as well as block-copolymer spots into mesoporous silica films using three different monomers was achieved with micrometer scale local resolution and spot sizes smaller than the irradiation laser beam size. Fluorescence Recovery after Photobleaching (FRAP) thereby provides insight into molecule diffusion in mesoporous silica films important for optimization of the polymer writing process.

2. Results and Discussion

A visible-light induced PET-RAFT was used for laser-based polymer writing into mesoporous silica thin films using the monomer 2-(dimethylamino)ethyl methacrylate (DMAEMA). In a first step, mesoporous silica films were prepared by dip coating using the evaporation-induced self-assembly (EISA).[36] Mesoporous silica films with a film thickness of ≈500 nm, porosity of 50–60 vol.% (Tables S5–S15, Supporting Information) and pore size of ≈13 nm (**Figure 1**b,c) were obtained. The mesoporous silica films were functionalized with a derivate of the RAFT agent DDMAT (2-(Dodecylthiocarbonothioylthio)-2-methylpropanoic acid) initiating the polymerization and polymer writing directly within the silica mesopores. Using the photo catalyst ZnTPP allows to initiate the polymerization under visible-light irradiation at 405 nm (Figure S1, Supporting Information). By using DMSO as solvent it is possible to perform the polymerization in an open vessel in the presence of oxygen, which is advantageous in the context of laser-induced polymer writing. Moreover, the PET-RAFT allows re-initiation and thus multi-functionalization because of its controlled radical polymerization character. The mesoporous structure remains intact even after polymerization for 2 h with a relatively high energy of 38 mW cm^{-2} (Figure 1c).

2.1. Polymerization Parameter Optimization for Polymer Writing in Mesopores

For efficient polymer writing a high polymer amount in short irradiation times while allowing spatially resolved polymer grafting is advantageous. To understand and optimize the reaction conditions in general and especially in mesoporous films, the influence of the RAFT agent DDMAT on the monomer conversion in solution was investigated by ^{1}H-NMR-spectroscopy
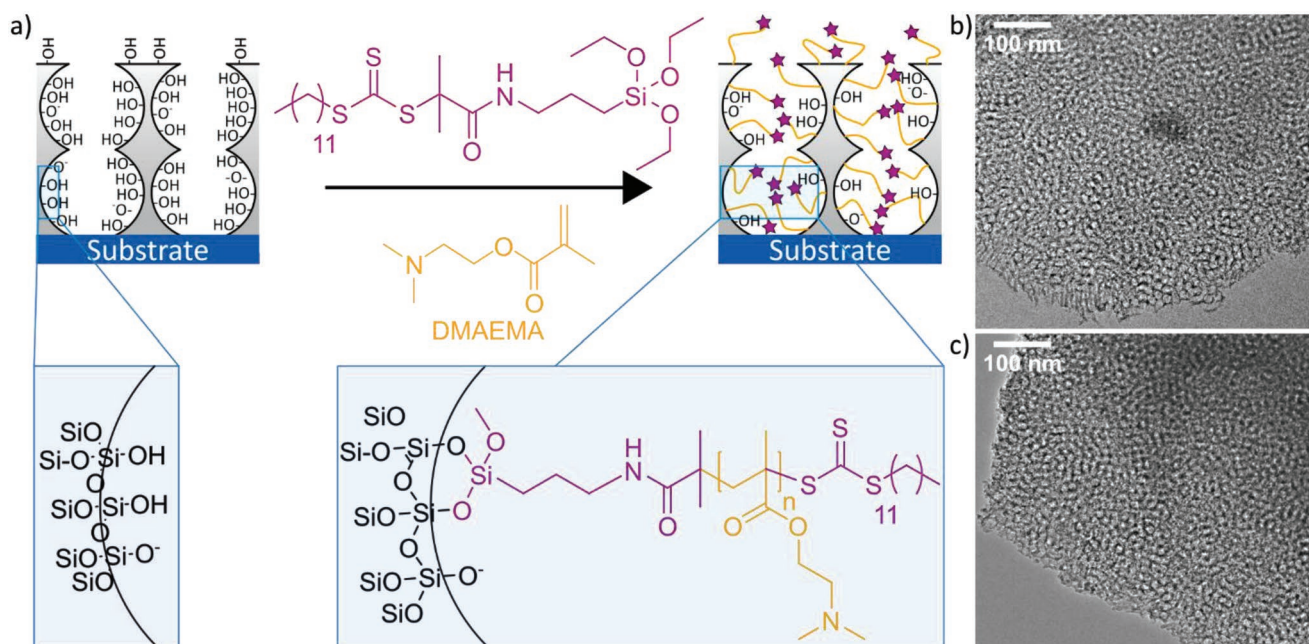
Figure 1. a) Schematic illustration of the visible-light induced mesopore functionalization using DDMAT as RAFT agent and DMAEMA as monomer. TEM images showing the mesoporous structure b) before and c) after visible-light induced polymerization of DMAEMA for 2 h at 38 mW cm^{-2}.

(Figures S1 and S2, Supporting Information). As expected, the highest monomer conversion was observed with the lowest DDMAT concentration of 2.4 mmol L^{-1} (Equation S2, Supporting Information). The influence of free DDMAT on polymerization in mesopores is consistent with the observation of reduced polymer amount in solution: using an irradiation energy of 2.5 mW cm^{-2} the presence of free DDMAT in the polymerization solution leads to a lower polymer amount grafted inside the mesoporous film as compared to a polymerization without free DDMAT (Figure S3a,b, Supporting Information). Besides, the presence and the concentration of free RAFT agent DDMAT an increasing monomer concentration leads to an increasing amount of grafted polymer within the mesoporous film (Figure S3a,b, Supporting Information). When performing the polymerization with and without free DDMAT at an irradiation energy of 38 mW cm^{-2}, using the monomer concentration of 2.9 mol L^{-1} ([DMAEMA]: [ZnTPP]: [DMSO (mL mg^{-1} ZnTPP)] = [500]: [0.025]: [10 mL]), the difference between polymerization with and without free DDMAT seems not to be significant at short irradiation times indicating monomer consumption through the formation of free polymer formation in solution. Besides being expected, solution polymerization leads to increasing viscosity of the polymerization solution with increasing irradiation time. Interestingly, the time-dependence of the generated polymer amount as detected by ATR-IR and TGA (Figure S3c,d, Supporting Information) is comparable to the time dependent polymer amount increase shown by the polymerization in solution (Figure S3a, Supporting Information). In mesopores, however, the time dependent increase of polymer amount does not seem to increase any further after about one hour polymerization time, whereas during polymerization in solution a significant time depended increase of polymer amount was observed until two to four hours reaction time. This is ascribed to the mesopore filling degree which reaches ≈88 vol.% after about one hour irradiation time using 38 mW cm^{-2} (Table S7, Supporting Information).

The polymer amount within the mesopores can be adjusted by varying the irradiation intensity and the irradiation time (**Figure 2**). The influence of irradiation intensity was analyzed without free DDMAT to achieve higher polymer pore filling already for short irradiation times which is advantageous for polymer writing. To differentiate the role of the outer planar mesoporous film surface from the inner pore wall functionalization a CO$_2$ plasma treatment[37,38] was used destroying the initiator at the outer planar surface of the mesoporous film.

For CO$_2$ plasma treated mesoporous films, and thus for polymerization exclusively occurring within the mesopores, the grafted polymer amount linearly increases up to a polymerization time of approximately 60 min under the applied conditions, using a relatively high irradiation intensity of 38 mW cm^{-2} (Figure 2a,b, black). For even longer irradiation times the polymer amount does not increase significantly further as the pores have been filled with polymer (Figure S4, Supporting Information). The stability of the mesoporous silica films when irradiated with 38 mW cm^{-2} was demonstrated by SEM and ellipsometry measurements (Figure S4a; Tables S5–S15, Supporting Information). When irradiating with a lower intensity of 2.5 mW cm^{-2}, the time dependent polymer amount increase changes (Figure 2a,b, blue): up to irradiation times of approximately 20 minutes almost no polymer is grafted to the mesopore wall indicating an induction period for the polymerization inside the mesoporous film. At a polymerization time of approximately 30 minutes polymer grafting starts following an almost linear increase of the grafted polymer amount with reaction time up to high pore filling degrees. Nevertheless, a much smaller polymer amount grafted per time is observed as compared to time dependent polymer amount
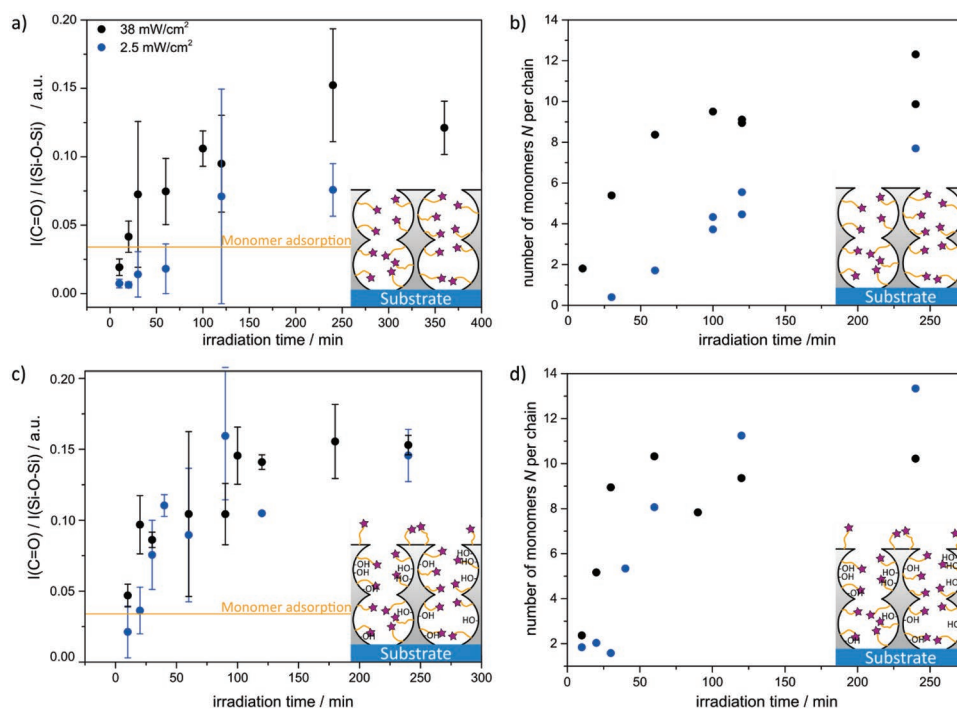
Figure 2. Influence of different irradiation intensities and polymerization times on the polymer amount in mesoporous silica films a,b) with and c,d) without CO_2 plasma treatment. a) The intensity of the carbonyl vibrational band (1725 cm^{-1}) relative to the Si—O—Si vibrational band (1060 cm^{-1}) for CO_2 plasma treated mesoporous films analyzed by ATR-IR spectroscopy. Mesoporous films were scratched off with a razor blade. Spectra were baseline corrected and normalized to the Si—O—Si-VS at 1060 cm^{-1}. The orange line represents the maximal carbonyl intensity reached by monomer adsorption without any polymerization reaction. b) Number of monomers per chain as deduced from TGA measurements for CO_2-plasma treated mesoporous films. The calculation of the number of monomers N per chain was carried out according to literature.[39] c) The intensity of the carbonyl vibrational band (1725 cm^{-1}) relative to the Si—O—Si vibrational band (1060 cm^{-1}) for mesoporous films without CO_2 plasma treated as deduced from ATR-IR spectroscopy in accordance to (a). d) Number of monomers per chain as deduced from TGA measurements for mesoporous films without CO_2-plasma treatment in accordance to (b). The error bars in Figure 2a,c, which shows the results of ATR-IR measurements, are based on multiple performance of the polymerization-experiment explaining partly high error bars.

increase at higher irradiation intensity. The rapid increase of polymer amount with increasing irradiation intensity as well as the existence of an induction period for this type of polymerization at relatively low irradiation intensity is in accordance with a previous study for solution polymerization and UV-light irradiation.[40] This study reports an induction period of around 50 minutes at an irradiation intensity of 3 mW cm^{-2} which was decreased to almost 0 minutes at 48 mW cm^{-2} being in accordance with our observations for polymerization in mesopores.

In case of polymer grafting inside the mesopores as well as on the outer planar mesoporous film surface (no CO_2 plasma treatment) differences between the two irradiation intensities decrease, and a linear increase in grafted polymer amount up to a polymerization time of about 60–100 minutes is observed. Considering the time-dependent polymer amount increase for polymer grafting inside the mesopores this indicates a significantly facilitated polymer functionalization at the outer mesoporous film surface which is consistent with previously reported polymer grafting approaches.[41]

TGA measurements using up to three independently functionalized mesoporous films in one measurement reveal a polymer chain length of up to ≈12 monomers per chain inside the mesopores (CO_2-plasma treated films). The estimated number of monomers N per chain is based on the assumption that every grafted DDMAT molecule starts a growing polymer chain and all chains are identically involved in the polymerization. Refractive index increase upon polymer grafting detected by ellipsometry and pore filling as determined using Brüggemann effective medium theory[42,43] reveal pore filling degrees up to 91 vol.% which are consistent with results from ATR-IR and TGA (Figure S4b, Supporting Information).

It is interesting to note that the mentioned time-dependent grafted polymer amount increase within the mesopores as well as the number of monomers N per chain up to high pore filling degrees indicates an ongoing exchange between mesopores and monomer solution during the polymerization as the final polymer amount seems to be larger than the initially adsorbed monomer concentration inside the mesopores indicated by a yellow line in Figure 2. The adsorbed monomer amount was deduced from ATR-IR spectra upon mesoporous film incubation into the polymerization solution and comparison of the subsequently detected C=O vibrational band intensity at 1710–1720 cm^{-1} in Si—O—Si (≈1060 cm^{-1}) spectra with the corresponding C=O vibrational band intensity after polymerization (Tables S3 and S4, Supporting Information). Consequently, the diffusion of monomer within the mesopores as well during polymerization seems to be an important aspect for the polymer functionalization and polymer writing.
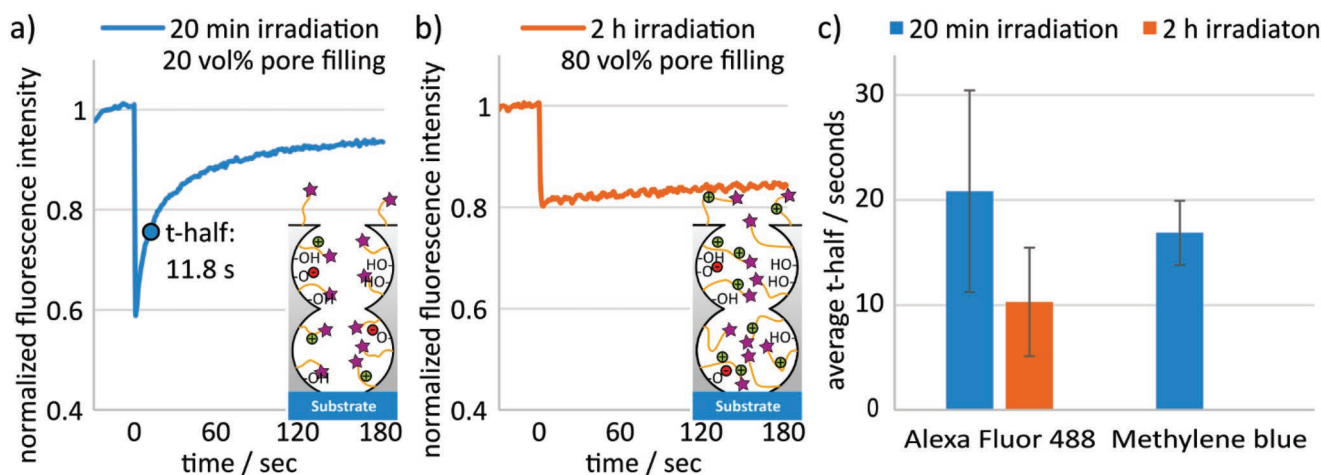
Figure 3. FRAP measurements shown exemplarily for a) PDMAEMA functionalized with 20 min irradiation time (20 vol.% pore filling) and b) PDMAEMA functionalized with 2 h irradiation time (80 vol.% pore filling) mesoporous silica film using positively charged methylene blue as fluorophore. Values for t-half could only be determined for 20 min irradiation time. c) Average values of t-half of FRAP measurements in PDMAEMA functionalized films using negatively charged Alexa Flour 488 and positively charged methylene blue as dye.

As a model component, the diffusion of positively charged methylene blue (MB) and negatively charged Alexa Fluor 488 fluorophores in PDMAEMA functionalized mesoporous silica films was investigated using fluorescence recovery after photobleaching (FRAP). The PDMAEMA polymerization of the mesoporous silica film was performed using an intensity of 38 mW cm^{-2} for 20 and 120 min to achieve two different PDMAEMA pore filling degrees of ≈20 and 80 vol.% (Figure S4, Supporting Information) and an estimated number of 5 and 9 monomers per chain (Figure 2b). The PDMAEMA functionalized films were incubated in dye containing (0.1 mg L^{-1}) aqueous solution for 30 minutes before the FRAP experiment was initiated. The pre-incubation was used to ensure equilibrium fluorophore concentration in the mesopores and remove any additional concentration gradient contributing to the fluorescence recovery. The dye recovery was analyzed and t-half, the time it takes to reach 50% recovery, was calculated (**Figure 3**). Using PDMAEMA functionalized films with a lower pore filling degree of ≈20 vol.% (20 minutes irradiation time, ≈5 monomers per chain according to Figure 2d) a t-half of 11.8 s for MB was determined for basic pH conditions (Figure 3a). Determining the t-half of MB recovery in films with a high PDMAEMA pore filling (80 vol.% pore filling) was not possible because only a slight staining of the film was observable which led to very low photobleaching. This resulted in a slow recovery and no steady state was reached in the observed time frame of up to 180 s (Figure 3b). Overall, values for t-half between 20.8 s for Alexa Fluor 488 at lower pore filling and 10.3 s at high pore filling degrees were determined, while methylene blue showed an average t-half of 16.9 s for lower pore filling of ≈20 vol.% (Figure 3c). This indicates significant diffusion of molecules inside of the mesopores which seems to be strongly dependent on the degree of pore filling. We suspect that the main diffusion inhibiting force is electrostatic interactions between the charged fluorophore and potentially negatively charged silica surface (non-functionalized) or potentially positively charged polymer inside the pores. The introduction of positively charged polymer inside the pores probably results

in a neutralization of the charge, allowing for diffusion of fluorophores in slightly filled pores, while in the case of MB, the strong similar charge in highly filled pores leads to an exclusion of the fluorophore. Using negatively charged Alexa Fluor 488 and varying PDMAEMA amount, a fluorescence recovery, indicating the diffusion of Alexa Fluor 488 molecules inside the mesopores, was observed. The fast recovery in highly filled pores also indicates that the charge of the pore plays a more important role in determining diffusion into the pore than steric hindrance due to high polymer content.

Ultimately, diffusion is possible even in highly filled pores (80 vol.%) when electrostatic conditions do not prevent it. Diffusion of monomers into the mesopores upon progressing polymerization time is thus feasible, allowing for potential re-initiation in polymer writing and high pore filling degrees in consistence with the above ATR-IR results (Figure 2).

2.2. Polymer Writing in Mesopores

Based on the developed understanding of the PET-RAFT in mesopores, a process for automated microscope-based polymer writing in mesoporous films was developed. Using the illumination laser of a commercially available microscope (Nikon Ti2-E with N-STORM unit) we wrote PDMAEMA with a micrometer scale pattern into mesoporous films. Furthermore, polymer writing is not limited to PDMAEMA, polymer writing of poly[2-(methacryloyloxy)-ethyl]-trimethylammoniumchloride (PMETAC) and poly-2-(methacryloyloxy)ethyl phosphate (PMEP) into mesoporous silica films was successfully implemented as well as polymerization re-initiation. Using a laser wavelength of 405 nm, a laser power set to 25 mW, and an illumination time of 120 s for each illuminated spot. The laser diameter was adjusted to ≈72 µm (1/e^2). Due to losses in the optical path, the power the laser is set to a higher power than it has after the objective. The actual measured laser power at the sample stage is listed in the (Table S15, Supporting Information). Using different monomers, we demonstrate polymer writing by writing lines with a

diameter of each PDMAEMA spot in the range of 26 µm, each PMETAC spot in the range of 55 µm and each PMEP spot in the range of 40 µm while using the mentioned identical irradiation conditions for each monomer (**Figure** 4a). The differences in polymer spot diameters could be of multiple origin including differences in charge, viscosity, monomer solubility, refractive indices, or polymerization kinetics of the used monomers under the given conditions. By staining the positively charged PMETAC (strong polyelectrolyte), and PDMAEMA (pKa value in solution ≈pH 7.5)[44] with negatively charged Alexa Fluor 488 at pH 4, the local PMETAC and PDMEAMEA polymer functionalization was visualized by fluorescence imaging. Using positively charged methylene blue (MB) solution at pH 7 the local functionalization of negatively charged PMEP (pKa values in solution ≈4,5 and 7,7)[45] was visualized (Figure 4).

Re-initiation of the polymerization during polymer writing was demonstrated by PDMAEMA writing followed by PMEP writing with overlapping illumination patterns (Figure 4b). For PDMAEMA, a cross-shaped pattern was written. The PMEP functionalization was performed with a square-shaped illumination pattern partly overlapping with the PDMAEMA pattern to re-initiate the polymerization in these locations. Illumination time, laser power, and wavelength were kept constant at 120 min, 25 mW, and 405 nm. The successful re-initiation of MEP polymerization in PDMAEMA functionalized spots of the mesoporous silica film is clearly detected in the overlapping regions (Figure 4b). Staining of the PDMAEMA in these regions was not possible which is ascribed to the negative charge of the PMEP being dominant in the PDMAEMA and PMEP dual-functionalized spots.
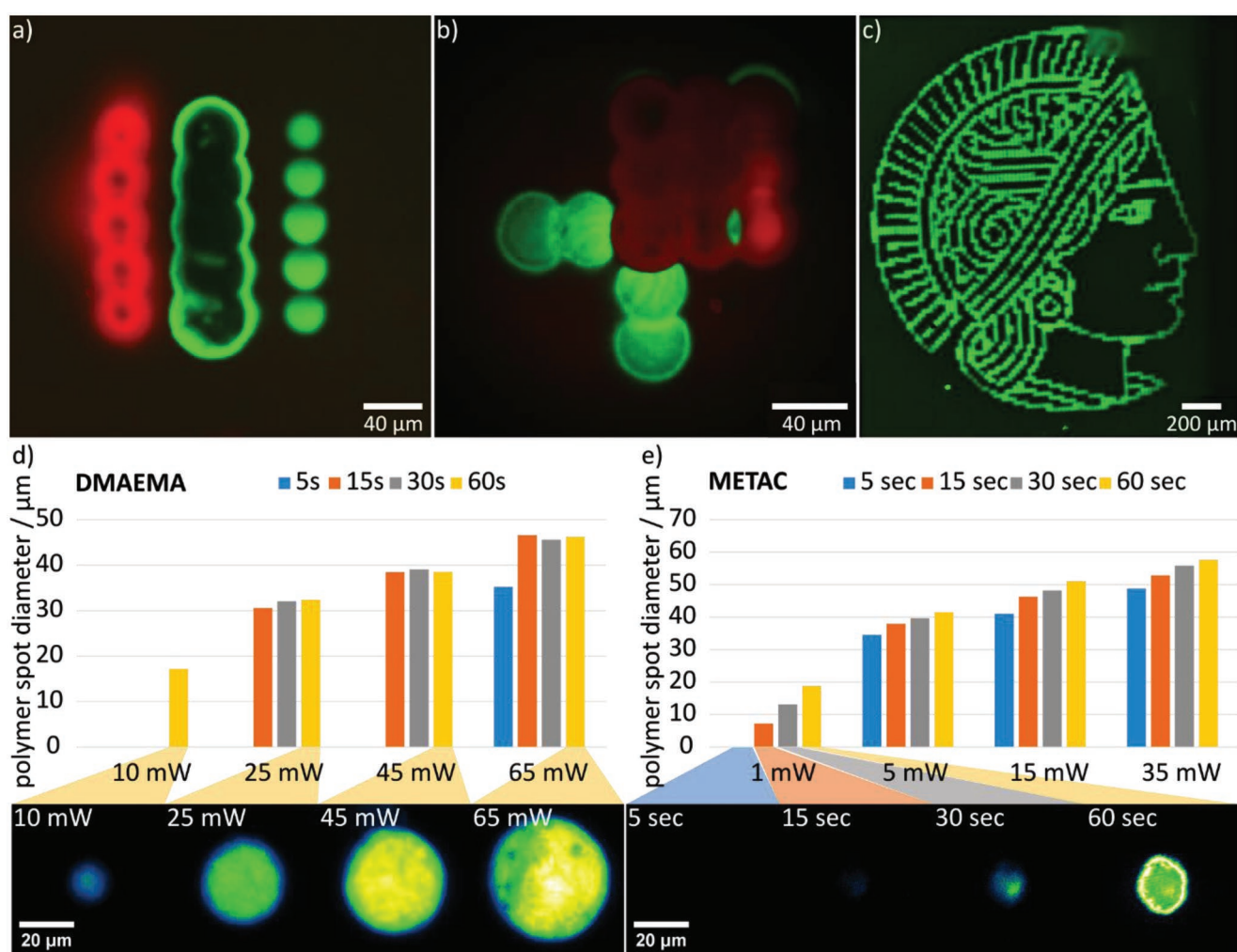

Figure 4. Visualization of local polymer functionalization in mesoporous silica films. In a,b) the DDMAT-functionalized film was irradiated for 120 s using a 405 nm laser at 25 mW. Staining was performed with Alexa Fluor 488 (green) at pH 4 and methylene blue (red) at pH 7. a) Shows a subsequent polymerization of PDMAEMA (right), PMETAC (middle), and PMEP (left). b) Shows a re-initiation of polymerization of PMEP in a PDMAEMA functionalized mesoporous silica film. First, a spot (top right) and a cross-shaped irradiation pattern was used for PDMAEMA polymerization. Then, a square-shaped irradiation pattern was used to re-initialize PMEP polymerization. Samples were washed for 30 min between polymerization steps and an incubation in polymerization solution for 30 min before irradiation was performed. In (c) an example for the printing of a complex pattern, representing a black and white pixel image is shown. In (d,e) tuning of polymer spot diameter while laser induced polymer writing at 405 nm is shown. d) Using DMAEMA as monomer the DDMAT-functionalized mesoporous silica film was functionalized using laser powers between 10 and 65 mW for 5–60 s. e) Using METAC as monomer the DDMAT-functionalized mesoporous silica film was functionalized using laser powers between 1 and 35 mW for 5–60 s.

To demonstrate the flexibility of the shape and size of this polymer writing approach, a (scaled down) pixel image of the TU Darmstadt Logo "Athene" with a size of 104 × 104 pixels, was applied for polymer writing in a mesoporous thin film (Figure 4). The black pixels in the image were automatically translated into a *xy*-position containing .xml file which can be directly loaded into the Nikon Elements software. The position corresponding to each black pixel was then illuminated for 1 second with a laser power set to 5 mW using METAC as monomer which led to polymer spots with a diameter of ≈30 μm. The illumination took ≈40 minutes and the spacing between illuminated positions was set to 20 μm. Overall, the resulting pattern was ≈2×2 mm in size. The polymer pattern was stained with Alexa Fluor 488 for imaging showing the successfully written PMETAC functionalization into the mesoporous silica film. The written polymer spot size can be adjusted by changing the diameter of the illumination laser. Furthermore, the dimensions of the written polymer can be tuned using the laser power and irradiation time. Consequently, a written polymer spot with a diameter significantly smaller than the diameter of the used illumination beam can be obtained. Using the 405 nm laser with a diameter of 72 μm ($1/e^2$) to write PDMAEMA into mesoporous films, we achieved the smallest polymer spot with a diameter of ≈17 μm when using a laser power of 10 mW for 60 seconds (Figure 4d). Shorter irradiation times at 10 mW did not result in detectable PDMAEMA polymer amount using fluorescence imaging for PDMAEMA detection. While using the same irradiation time of 60 seconds, but increasing laser power from 10 to 65 mW the PDMAEMA spot size also increased up to a diameter of ≈46 μm. An increasing polymer amount at the same irradiation time, but with higher energy is consistent with ATR-IR and TGA data on PDMAEMA functionalization on larger scale (Figure 2). For the laser induced polymerization using METAC less energy was required to observe polymer grafting. Using a laser power of 1 mW for only 15 seconds a polymer spot in the range of 7 μm diameter was obtained (Figure 4e). At constant laser power and increasing irradiation time, an increase of the PMETAC spot size is observed, which again agrees with the PDMAEMA functionalization of mesoporous silica films at larger scale.

Based on this parameter screening it is possible to create a multiple stimuli-responsive polymer writing into mesoporous silica thin films with a lateral micrometer resolution. The use of a commercially available microscope made automation easy and opened basically any (binary) image for polymer writing into mesoporous films as demonstrated on the example of the "Athene" with a polymer spot size or 30 μm and an overall size of 104×104 pixels spots⁻¹ (Figure 4c). This highly flexible approach allows for rapid prototyping, speeding up product development and research. Moreover, inspired by our previous work on polymerization re-initiation in mesopores,[46] polymer re-initiation while writing PDMAEMA with a micrometer-scale pattern and subsequent writing of PMEP upon re-initiation on to the same spot was demonstrated (Figure 4b). This shows the potential of re-initiation to allow the creation of block-copolymers inside the mesoporous silica thin film. Consequently, we demonstrate a strategy to design millimeter-scale polymer written images with micrometer-scale resolution consisting of different polymers combined or even using re-initiation being generated in an automated fashion into mesoporous films using the illumination laser and optics of a commercially available microscope for visible light-based polymer writing. This opens manifold automated design strategies of multifunctional mesoporous materials.

3. Conclusion

We demonstrate automated, micrometer-scale resolution, and polymer writing of different stimuli-responsive polymers, such as PDMAEMA, PMETAC, and PMEP into mesoporous silica layers using a commercially available microscope (Nikon Ti2-E with N-STORM unit). A key step to this polymer writing in mesoporous films was the successful transfer of the oxygen tolerant, visible-light induced PET-RAFT, with DDAMAT as RAFT reagent, to mesoporous silica thin film polymer functionalization. A tunable polymer amount inside the mesoporous film was achieved by modulating irradiation energy, irradiation time, and by the addition of free RAFT agent, especially at shorter polymerization times up to 60 minutes. At high pore filling degrees of ≈90 vol.% a number of monomers *N* per chain of up to 12 monomers per chain was estimated. The obtained high pore filling degrees in combination with incubation reference experiments and FRAP measurements indicate existing monomer diffusion even during polymerization resulting in high polymer pore filling degrees. When using the illumination laser with a diameter of ≈72 μm, the written polymer spot size was optimized and tuned down to 7 μm in diameter by adjusting polymer type (PMETAC), laser power (1 mW), and irradiation time (15 seconds). The minimum irradiation time per polymer spot was optimized down to 1 second per spot, without further forcing toward shorter irradiation times, enabling reasonable writing times for larger and more complex images. A shorter illumination time of down to 0.25 seconds was achieved in initial tests (data not shown), showing further potential for optimization. Additionally, the capability to write multiple monomers into a block-copolymer multipolymer microscale image through polymerization re-initiation with micrometer scale local control in mesoporous materials was demonstrated. This automated polymer writing in porous materials including polymer re-initiation opens a new avenue for porous material fabrication which is of relevance especially in fabrication of mesoporous material devices for high throughput applications in machine learning coupled sensing, medicine and Lab on a Chip devices. Going toward high throughput applications the further optimization of writing speed will be addressed in future work.

4. Experimental Section

Chemicals: Pluronic F127, 2-(dodecylthiocarbonothioylthio)-2-methylpropionic acid (98%, HPLC), ethanol (absolute EMPLURA), dichlormethane (anhydrous, ≥99.8%), 5,10,15,20-tetraphenyl-21*H*,23*H*-porphine zinc (ZnTPP), APTES (≥ 98%), dimethylaminoethyl methacrylate (DMAEMA, 98%), *N*-(3-dimethylaminopropyl)-*N'*-ethylcarbodiimid–hydrochlorid (EDC-HCl), methylene blue (MB), and tetraethylorthosilicate (TEOS) (98%, reagent grade) had been purchased from Sigma–Aldrich/Merck. The monomer DMAEMA was destabilized

over a γ-aluminium column before use. Toluene (anhydrous, 99.8%) was purchased from Alfa Aesar and DMSO (99%) from Grüssing GmbH. Alexa Fluor 488 (A30629) was purchased from ThermoFisher Scientific.

Mesoporous Silica Thin Films: The preparation of the mesoporous silica thin films were carried out using sol-gel chemistry and evaporation induced self-assembly. The amphiphilic triblock copolymer Pluronic F127 was used as mesopore template and tetraethylorthosilicate (TEOS) as inorganic precursor. Inspired by Dunphy et al.[47] a dip-coating process were performed to produce mesoporous silica films with pore sizes of ≈16 nm and film thicknesses of ≈500–600 nm. For the dip-coat solution 9,8 mL TEOS were dissolved in 48,0 mL ethanol. Then 5,22 g Pluronic F127 and 12,8 mL of a freshly prepared hydrochloric acid solution (0,05 м) were added. The solution was stirred for 1 h at room temperature and stored in the freezer (−18 °C) till use.

The formation of the mesoporous silica thin films were realized by Evaporation-Induced Self-Assembly (EISA).[36] Glass substrates, ITO-coated glass substrates, and silicon wafers were washed with ethanol and dip-coated using a withdrawal speed of 2 mm s⁻¹ under controlled environmental conditions in a climate-controlled chamber (Binder APT. lineTM KBF, E5.2) at 40–50% rel. humidity and 25 °C. The films were stored under these conditions for at least 1 h before the following temperature treatment was carried out: heating up to 60 °C within 10 min and holding the temperature for 60 min, followed by a temperature increase up to 130 °C within 10 min, and holding the temperature at 130 °C for 60 min. Subsequently heating to 350 °C using a heating rate of 1 °C min⁻¹ and keeping this temperature for 2 h was carried out.

Surface Grafting of DDMAT: For grafting the RAFT-agent DDMAT on the mesoporous silica film the DDMAT had to be modified with a silica-anchor according to the literature.[9] Briefly, under nitrogen atmosphere 1 mmol DDMAT was dissolved in 50 mL dry dichloromethane (DCM). In another flask 1 mmol EDC HCl was dissolved in 10 mL dry DCM. Then the EDC HCl solution was added dropwise into the first flask. The solution was cooled and stirred at 0 °C before 1 mmol APTES was added dropwise. The yellow/orange reaction solution was stirred for 2 h at 0 °C and after that for another 2 h at room temperature. The solution was concentrated using a rotary evaporator (40 °C). Silica gel column chromatography (1:1 v/v EE and cyclohexene) R_f(DDMAT-derivate) = 0,92. ¹H NMR (300 MHz, CDCl₃, δ, ppm): 0.559 (t, 2H), 0.866 (t, 3H), 1.207 (t, 9H), 1.284 (m, 18H), 1.602 (m, 4H), 1.679 (s, 6H), 3.228 (m, 2H), 3.787 (t, 6H), and 6.605 (t, 1H) (see previous study).[35]

The grafting of the modified RAFT agent DDMAT and the following polymerizations were carried out on mesoporous silica thin films using three different substrates. Glass substrates, Indium-thin-oxide (ITO)-coated glass substrates, and silicon (Si)-wafers. To functionalize the films a solution of 2.4 mmol L⁻¹ DDMAT-derivate (DDMAT with silica-anchor) in dry toluene was prepared and filled into a Schlenk tube, which contained substrates with mesoporous silica films under exclusion of oxygen. The Schlenk tube was heated in a water bath (80 °C) for 1 h. Subsequently, the substrates were washed with toluene and ethanol.

PDMAEMA Functionalization of Mesoporous Silica Films via PET-RAFT: Inspired by the group of Pester,[9] the polymer functionalization of the mesoporous silica films were performed by a PET-RAFT using visible light. As photo catalyst ZnTPP and as solvent DMSO was used. For the polymerization DDMAT-functionalized silica films were placed in tubes with contained a solution with the following molar ratio, if not other mentioned = [monomer]: [ZnTPP]: [DMSO (mL per mg ZnTPP)] = [500]: [0.025]: [10 mL]. The polymerization was initiated by visible-light irradiation using a lamp (LUMATEC Superlite 400, 400–700 nm filter, 2.5, or 38 mW cm⁻²) for different irradiation times. After irradiation, the residual monomer was extracted in water for at least 10 min.

PDMAEMA Functionalization in Solution via PET-RAFT: The PET-RAFT in solution was performed in analogy to the polymerization in mesoporous silica films, however, without substrate with mesoporous silica film inside of the flask and in solution polymerization additional RAFT agent DDMAT (2.4, 3.0, and 5.9 mmol L⁻¹) was present. Moreover, the polymerization solution was stirred during irradiation. After various irradiation times (30 min, 1 h, 4 h, and 6 h) samples were taken, diluted with H₂O and analyzed by ¹H-NMR spectroscopy.

ATR-IR Spectroscopy: IR spectra were recorded in the attenuated total reflection (ATR) mode using a Spectrum One Fourier transform infrared (FT-IR) spectrometer from PerkinElmer in the range from 4000–650 cm⁻¹. The films were scratched off with a razor blade. The recorded data was background-corrected by the software. Also the spectra were baseline corrected and normalized to the Si—O—Si asymmetric stretching vibrational band at ≈1060 cm⁻¹ using OriginPro9.

For polymer amount analysis ATR-IR spectra were recorded for polymerization at 2.5 or 38 mW cm⁻² and for irradiation times between 10 and 240 min, with and without additional DDMAT. The resulting spectra were automatically baseline corrected and normalized to the Si—O—Si vibrational band at ≈1060 cm⁻¹. Information on the polymer amount were obtained by comparing the vibrational band from the PDMAEMA carbonyl group at 1720–1730 cm⁻¹ after varying polymerization conditions in these normalized ATR-IR spectra.

Ellipsometry: The determination of refractive indices and film thicknesses was carried out by ellipsometry on silicon wafer substrates (Si-Mat, Kaufering, Germany, 100 mm diameter, 525 ± 25 µm thickness, type P/Bor, <100> orientation, CZ growth method, 2–5 W resistivity, polished on 1 side) using the device nanofilm EP3-SE (ACCURION) with a 658 nm laser. As software EP4-View and EP4-model (version 1.2.0) was used for measurement and model analysis. For the measurements an angle range of 38°–70° in 2° increments were used and was performed at three measuring points along the pulling direction of the dip coating and measured in one-zone mode (Si-wafer→SiO₂-oxide layer→SiO₂ mesoporous). With the program Regul'Hum (version 3.3) a relative humidity of 15% was adjusted to exclude water condensation inside the mesopores. The calculation of pore fillings was carried out according to Bruggeman effective medium theory[42,43] by using the refractive indices. For the calculation of PDMAEMA pore filling n = 1.517[48] for PDMAEMA was used unless otherwise noted. For all organic molecules n = 1.5 was assumed.

CO₂-Plasma Treatment: The CO₂-plasma treatment was performed with a Diener Electronic 20 Femto plasma system analogous to Krohm et al.[37] and Babu et al.[38] at a pressure of 0.3 mbar and a power off 20% (10 W). The duration was 12 s.

TGA Measurements: The TGA measurements were performed on the TGA 1 STARe System from Mettler Toledo with the software STARe Software, version 12.10b (Build 6401). The following temperature treatment was carried out using an air flow of 30 mL min⁻¹: heat up from 25 to 100 °C in 10 K min⁻¹ and hold the temperature for 15 min, heat up to 600 °C in 10 K min⁻¹. For the measurement 100 µL aluminium-crucibles were used. The sample mass was between 0.23 and 1.15 mg. Determination of the grafting density and number of monomers N per chain were done by using the following Equations 1–3.[39] W% was the weight loss from TGA measurements, G_I was the grafting density of the RAFT agent DDMAT, G_P the polymer grafting density and S_{sp} the specific surface.

$$G_I \left(\frac{molecule}{nm^2} \right) = \frac{\frac{W\%_{silica+Initiator}}{100 - W\%_{silica+Initiator}} - \frac{W\%_{silica}}{100 - W\%_{silica}}}{M_{Initiator} \cdot S_{sp}} \cdot N_A \tag{1}$$

$$G_I = G_P \tag{2}$$

$$M_P = \frac{\frac{W\%_{silica+polymer}}{100 - W\%_{silica+polymer}} - \frac{W\%_{silica+Initiator}}{100 - W\%_{silica+Initiator}}}{G_P \cdot S_{sp}} \cdot N_A \tag{3}$$

Microscope: For all experiments involving a microscope (FRAP, laser polymer writing, and fluorescence imaging) a Nikon Eclipse Ti2-E (Nikon, Tokyo, Japan) equipped with an N-Storm and FRAP module was used. Three laser lines with wavelength of 405, 488, and 638 nm were connected to either the N-STROM or the FRAP module. For epi-illumination a Nikon Sola solid-state white light source was used. A CFI Apo TIRF 60XC Oil (MRD01691) was used as objective. An Andor ZYLA 4.2 PLUS (Andor Technology, Belfast, UK) was used for image

acquisition. The setup was controlled using the NIS-Elements (version 5.20) software.

Laser Polymer Writing: To initiate the photopolymerization, the 405 nm illumination laser was used. A beam expander setting of "8x" in combination with the 60x objective resulted in a laser spot size of ≈72 μm ($1/e^2$) in diameter. Polymer "writing" was achieved by using the built-in macro function to loop over a list of *xy*-positions with the motorized sample stage and opening the laser illumination shutter for a specified time at each position. The list was created with a custom written Python script, translating the black pixel of a black and white pixel image into *xy*-positions. The distance between the *xy*-positions need to be specified by hand. This way a representation of the pixel image could be "printed" onto a sample.

The sample consisting of a mesoporous thin film prepared on a 2.5 mm diameter, 170 μm thick, No 1.5, round microscopy borosilicate cover glass (VWR International, Radnor, Pennsylvania, US). It was placed with the thin film facing upward into a custom build stainless steel sample holder, which holds ≈1 ml of polymerization solution (Monomer, ZnTPP, DMSO) on top of the sample.

Local Polymerization Visualization: To visualize polymer functionalization with a fluorescence microscope, the polymer was stained with a fluorophore on the basis of electrostatic interactions. Charged polymer (PMETAC) was stained using oppositely charged fluorophore. For non-permanently charged polymers (PDMAEMA, PMEP), pH conditions were set accordingly to ensure a charge in the polymer to allow for staining with counter charged fluorophore. Alexa Fluor 488 was used as a negatively charged fluorophore to stain PMETAC and PDMAEMA, whereas methylene blue was used as a positively charged fluorophore to stain PMEP. For staining, a solution of 1 μg ml^{-1} fluorophore in water (pH 4 for Alexa Fluor 488 and pH 7 for methylene blue) was applied to the sample for 10 min, followed by a washing step in water (pH 7) for 30 min.

Images were acquired by epi-fluorescence imaging, using the in-built stitching function to acquire images bigger than the field a view.

FRAP Measurements: Bleaching was performed either with a 488 nm (Alexa Fluore 488) or a 638 nm (methylene blue) laser set to 50 mW. A 40×40 pixel sized square (≈300 μm^2) was bleached with a dwell time of 100 μs. Images before and after the bleaching were acquired using a TIRF configuration with 1 fps. The incidence angle was determined automatically through the NIS-Elements software for each sample. Data analysis was performed using the stand alone MatLab application of EasyFRAP.[52] In EasyFRAP, Roi 1 was set to the bleached region, Roi 2 was defined as the whole region illuminated by the laser, and Roi 3 was set to a 100×100 pixel square at the (non-illuminated) top right of the image. For normalization "double" was chosen and a "double term" fitting equation was used for the mean data of three measurements.

SEM Measurements: The SEM measurements were performed on the device Philips XL30 FEG with a SE detector, operated on an accelerating voltage of 20 kV and a working distance of ≈10 mm. Before SEM measurements the samples were fixed on the sample holder using conducting tape (copper) and coated with a 7 nm platinum/palladium layer using a Cression 208 HR Sputter Coater.

TEM Measurements: TEM measurements were performed on a JEOL JEM 2100F TEM with a resolution of 2.2 Å operating at an accelerating voltage of 200 kV. For sample preparation the mesoporous silicafilm were scratched off from the substrate, dispended in ethanol and placed in the ultrasonic bath for 3 min. The dispersion was dropped on a TEM grid and dried under ambient conditions.

^{1}H-NMR Spectroscopy: ^{1}H-NMR measurements were performed on DRX 300 from Bruker Biospin GmbH using 300 MHz as frequency. The chemical shift δ was given in parts per million (ppm). Analysis of the spectra were done with MestReNova (MestreLabResearch). All spectra were baseline corrected using the Bernstein polynomial fit and an automatic phase correction was done. The undertreated residual signals of the used solvents serve as a reference for the chemical shift for normalization of the signals obtained according to literature.[49] Also, the spectra were baseline and phase corrected.

Supporting Information

Supporting Information is available from the Wiley Online Library or from the author.

Conflict of Interest

The authors declare no conflict of interest.

Data Availability Statement

The data that support the findings of this study are available from the corresponding author upon reasonable request.

[1] a) Y. Temiz, R. D. Lovchik, G. V. Kaigala, E. Delamarche, *Microelectron. Eng.* **2015**, *132*, 156; b) Y. C. Lim, A. Z. Kouzani, W. Duan, *Microsyst. Technol.* **2010**, *16*, 1995; c) E. Reimhult, F. Höök, *Sensors* **2015**, *15*, 1635.

[2] R. Pardehkhorram, A. Andrieu-Brunsen, *Chem. Commun.* **2022**, *58*, 5188.

[3] J. Kimmig, S. Zechel, U. S. Schubert, *Adv. Mater.* **2021**, *33*, 2004940.

[4] S. Oliver, L. Zhao, A. J. Gormley, R. Chapman, C. Boyer, *Macromolecules* **2019**, *52*, 3.

[5] G. Ng, J. Yeow, R. Chapman, N. Isahak, E. Wolvetang, J. J. Cooper-White, C. Boyer, *Macromolecules* **2018**, *51*, 7600.

[6] a) R. Hoogenboom, U. S. Schubert, *J. Polym. Sci., Part A: Polym. Chem.* **2003**, *41*, 2425; b) R. Hoogenboom, M. A. R. Meier, U. S. Schubert, *Macromol. Rapid Commun.* **2003**, *24*, 15.

[7] Z. Nie, E. Kumacheva, *Nat. Mater.* **2008**, *7*, 277.

[8] M. Tamasi, S. Kosuri, J. DiStefano, R. Chapman, A. J. Gormley, *Adv. Intell. Syst.* **2020**, *2*, 1900126.

[9] M. Li, M. Fromel, D. Ranaweera, S. Rocha, C. Boyer, C. W. Pester, *ACS Macro Lett.* **2019**, *8*, 374.

[10] a) B. P. Fors, J. E. Poelma, M. S. Menyo, M. J. Robb, D. M. Spokoyny, J. W. Kramer, J. H. Waite, C. J. Hawker, *J. Am. Chem. Soc.* **2013**, *135*, 14106; b) Y. Tian, H. Notsu, T. Tatsuma, *Photochem. Photobiol. Sci.* **2005**, *4*, 598; c) J. E. Poelma, B. P. Fors, G. F. Meyers, J. W. Kramer, C. J. Hawker, *Angew. Chem., Int. Ed.* **2013**, *52*, 6844.

[11] J. Rühe, *ACS Nano* **2017**, *11*, 8537.

[12] J. del Barrio, C. Sánchez-Somolinos, *Adv. Opt. Mater.* **2019**, *7*, 1900598.

[13] a) S. Engelhardt, in *Biological and Medical Physics, Biomedical Engineering* (Eds: V. Schmidt, M. R. Belegratis), Springer, Berlin, Germany **2013**, pp. 13–65; b) C. Barner-Kowollik, M. Bastmeyer, E. Blasco, G. Delaittre, P. Müller, B. Richter, M. Wegener, *Angew. Chem.* **2017**, *129*, 16038.

[14] A. Selimis, V. Mironov, M. Farsari, *Microelectron. Eng.* **2015**, *132*, 83.

[15] M. Malinauskas, M. Farsari, A. Piskarskas, S. Juodkazis, *Phys. Rep.* **2013**, *533*, 1.

[16] R. Wollhofen, J. Katzmann, C. Hrelescu, J. Jacak, T. A. Klar, *Opt. Express* **2013**, *21*, 10831.

[17] a) B. Harke, P. Bianchini, F. Brandi, A. Diaspro, *ChemPhysChem* **2012**, *13*, 1429; b) J. B. Mueller, J. Fischer, F. Mayer, M. Kadic, M. Wegener, *Adv. Mater.* **2014**, *26*, 6566.

[18] S. Telitel, S. Telitel, J. Bosson, A. Spangenberg, J. Lalevée, F. Morlet-Savary, J.-L. Clément, Y. Guillaneuf, D. Gigmes, O. Soppera, *Adv. Mater. Interfaces* **2014**, *1*, 1400067.

[19] S. Telitel, J. C. Morris, Y. Guillaneuf, J.-L. Clément, F. Morlet-Savary, A. Spangenberg, J.-P. Malval, J. Lalevée, D. Gigmes, O. Soppera, *ACS Appl. Mater. Interfaces* **2020**, *12*, 30779.

[20] T. Tang, G. Ahumada, C. W. Bielawski, *Polym. Chem.* **2020**, *11*, 5437.

[21] X. Wu, B. Gross, B. Leuschel, K. Mougin, S. Dominici, S. Gree, M. Belqat, V. Tkachenko, B. Cabannes-Boué, A. Chemtob, A. Spangenberg, J. Poly, *Adv. Funct. Mater.* **2022**, *32*, 2109446.

[22] S. Telitel, F. Dumur, S. Telitel, O. Soppera, M. Lepeltier, Y. Guillaneuf, J. Poly, F. Morlet-Savary, P. Fioux, J.-P. Fouassier, D. Gigmes, J. Lalevée, *Polym. Chem.* **2015**, *6*, 613.

[23] H. M. Jin, S. H. Lee, J. Y. Kim, S.-W. Son, B. H. Kim, H. K. Lee, J. H. Mun, S. K. Cha, J. S. Kim, P. F. Nealey, K. J. Lee, S. O. Kim, *ACS Nano* **2016**, *10*, 3435.

[24] R. Brilmayer, C. Förster, L. Zhao, A. Andrieu-Brunsen, *Curr. Opin. Biotechnol.* **2020**, *63*, 200.

[25] S. Shanmugam, J. Xu, C. Boyer, *J. Am. Chem. Soc.* **2015**, *137*, 9174.

[26] a) M. Ciftci, M. A. Tasdelen, Y. Yagci, *Polym. Chem.* **2014**, *5*, 600; b) A. Bansal, A. Kumar, P. Kumar, S. Bojja, A. K. Chatterjee, S. S. Ray, S. L. Jain, *RSC Adv.* **2015**, *5*, 21189.

[27] a) Q. Michaudel, V. Kottisch, B. P. Fors, *Angew. Chem.* **2017**, *129*, 9798; b) J. V. Crivello, *J. Polym. Sci., Part A: Polym. Chem.* **1999**, *37*, 4241.

[28] P. Lu, N. M. Alrashdi, A. J. Boydston, *J. Polym. Sci., Part A: Polym. Chem.* **2017**, *55*, 2977.

[29] J. Xu, K. Jung, A. Atme, S. Shanmugam, C. Boyer, *J. Am. Chem. Soc.* **2014**, *136*, 5508.

[30] W. Wang, S. Zhong, G. Wang, H. Cao, Y. Gao, W. Zhang, *Polym. Chem.* **2020**, *11*, 3188.

[31] J. Xu, S. Shanmugam, H. T. Duong, C. Boyer, *Polym. Chem.* **2015**, *6*, 5615.

[32] S. Shanmugam, J. Xu, C. Boyer, *Angew. Chem., Int. Ed. Engl.* **2016**, *55*, 1036.

[33] P. N. Kurek, A. J. Kloster, K. A. Weaver, R. Manahan, M. L. Allegrezza, N. de Alwis Watuthanthrige, C. Boyer, J. A. Reeves, D. Konkolewicz, *Ind. Eng. Chem. Res.* **2018**, *57*, 4203.

[34] T. Joshi, L. Nebhani, *Surf. Interfaces* **2022**, *29*, 101764.

[35] C. Förster, L. Veith, A. Andrieu-Brunsen, *RSC Adv.* **2022**, *12*, 27109.

[36] C. J. Brinker, Y. Lu, A. Sellinger, H. Fan, *Adv. Mater.* **1999**, *11*, 579.

[37] F. Krohm, J. Kind, R. Savka, M. Alcaraz Janßen, D. Herold, H. Plenio, C. M. Thiele, A. Andrieu-Brunsen, *J. Mater. Chem. C* **2016**, *4*, 4067.

[38] D. J. Babu, S. Yadav, T. Heinlein, G. Cherkashinin, J. J. Schneider, *J. Phys. Chem. C* **2014**, *118*, 12028.

[39] P. Pasetto, H. Blas, F. Audouin, C. Boissière, C. Sanchez, M. Save, B. Charleux, *Macromolecules* **2009**, *42*, 5983.

[40] H. Wang, Q. Li, J. Dai, F. Du, H. Zheng, R. Bai, *Macromolecules* **2013**, *46*, 2576.

[41] L. Silies, H. Didzoleit, C. Hess, B. Stühn, A. Andrieu-Brunsen, *Chem. Mater.* **2015**, *27*, 1971.

[42] J. E. Spanier, I. P. Herman, *Phys. Rev. B* **2000**, *61*, 10437.

[43] C. Boissiere, D. Grosso, S. Lepoutre, L. Nicole, A. B. Bruneau, C. Sanchez, *Langmuir* **2005**, *21*, 12362.

[44] P. van de Wetering, N. J. Zuidam, M. J. van Steenbergen, O. A. G. J. van der Houwen, W. J. M. Underberg, W. E. Hennink, *Macromolecules* **1998**, *31*, 8063.

[45] A. Brunsen, C. Díaz, L. I. Pietrasanta, B. Yameen, M. Ceolín, G. J. A. A. Soler-Illia, O. Azzaroni, *Langmuir* **2012**, *28*, 3583.

[46] R. Brilmayer, C. Hess, A. Andrieu-Brunsen, *Small* **2019**, *15*, e1902710.

[47] D. R. Dunphy, P. H. Sheth, F. L. Garcia, C. J. Brinker, *Chem. Mater.* **2015**, *27*, 75.

[48] S. Gupta, M. Agrawal, M. Conrad, N. A. Hutter, P. Olk, F. Simon, L. M. Eng, M. Stamm, R. Jordan, *Adv. Funct. Mater.* **2010**, *20*, 1756.

[49] G. R. Fulmer, A. J. M. Miller, N. H. Sherden, H. E. Gottlieb, A. Nudelman, B. M. Stoltz, J. E. Bercaw, K. I. Goldberg, *Organometallics* **2010**, *29*, 2176.